Laser optoacoustic imaging system for detection of breast cancer

Sergey A. Ermilov
Fairway Medical Technologies, Inc.
9431 West Sam Houston Parkway South
Houston, Texas 77099

Tuenchit Khamapirad
The University of Texas Medical Branch
301 University Boulevard
Galveston, Texas 77555

Andre Conjusteau
Fairway Medical Technologies, Inc.
9431 West Sam Houston Parkway South
Houston, Texas 77099

Morton H. Leonard
The University of Texas Medical Branch
301 University Boulevard
Galveston, Texas 77555

Ron Lacewell
Ketan Mehta
Tom Miller
Alexander A. Oraevsky
Fairway Medical Technologies, Inc.
9431 West Sam Houston Parkway South
Houston, Texas 77099

Abstract. We designed, fabricated and tested the laser optoacoustic imaging system for breast cancer detection (LOIS-64), which fuses optical and acoustic imaging techniques in one modality by utilizing pulsed optical illumination and ultrawide-band ultrasonic detection of resulting optoacoustic (OA) signals. The system was designed to image a single breast slice in craniocaudal or mediolateral projection with an arc-shaped array of 64 ultrawide-band acoustic transducers. The system resolution on breast phantoms was at least 0.5 mm. The single-channel sensitivity of 1.66 mV/Pa was estimated to be sufficient for single-pulse imaging of 6 to 11 mm tumors through the whole imaging slice of the breast. The implemented signal processing using the wavelet transform allowed significant reduction of the low-frequency (LF) acoustic noise, allowed localization of the optoacoustic signals from tumors, and enhanced the contrast and sharpened the boundaries of the optoacoustic images of the tumors. During the preliminary clinical studies on 27 patients, the LOIS-64 was able to visualize 18 out of 20 malignant lesions suspected from mammography and ultrasound images and confirmed by the biopsy performed after the optoacoustic tomography (OAT) procedure. [DOI: 10.1117/1.3086616]

Keywords: near-infrared (NIR) spectroscopy; optoacoustic tomography (OAT); breast ultrasound; mammography; tumor angiogenesis.

Paper 08230RR received Jul. 11, 2008; revised manuscript received Jan. 7, 2009; accepted for publication Jan. 7, 2009; published online Mar. 6, 2009.

1 Introduction

Imaging of breast cancer has been a field of significant advances in recent years. However, none of the imaging technologies could demonstrate sensitivity and specificity of breast cancer detection, that would be sufficient for standalone application.[1–3] Usually, mammography is combined with ultrasound to improve the detection outcome.[1] The emerging modalities of optical tomography combined with various spectroscopic tumor characterization strategies[4–6] and magnetic resonance imaging (MRI)[7,8] could provide additional information on blood distribution in the tumor microvasculature related to angiogenesis and aggressive growth of malignancy.

The laser optoacoustic imaging system (LOIS) of breast cancer was proposed over a decade ago as a new high-resolution method based on time-resolved ultrasonic signals generated in tissue by short laser pulses.[9] Initial works stimulated further research dedicated to this important medical application of optoacoustic tomography (OAT).[10–16] OAT of breast cancer takes advantage of the enhanced optical absorption of blood-rich tumors[17,18] and relatively high optical transparency of normal tissues[19] in the near-infrared (NIR) optical range. Optical absorption of a short NIR laser pulse increases internal thermal energy in tissues with enhanced absorption coefficient, such as breast tumors. The resultant local mechanical stress is dissipated through propagating ultrasonic waves. The temporal pressure confinement is the important requirement allowing OAT.[20] It assumes that the laser pulse is much shorter than the time it takes for the generated ultrasound to escape from the volume with characteristic dimension equal to the desirable spatial resolution. For human tissues, the speed of sound is $c_s \approx 1.5$ mm/μs. Therefore, the laser pulse must be much shorter than 333 ns to achieve spatial resolution of 0.5 mm or better.

Several techniques have been implemented to solve the inverse (tomography) problem of optoacoustic (OA) image reconstruction. For a single absorptive object that has a simple shape, e.g., a spherical shape, the exact analytical solution of the OA wave equation can be used to relate the magnitude of the OA pressure signal to the absorption coefficient.[21,22] For more complex irregular geometries and multiple objects, statistical methods based on a linear regression model have been shown to provide reliable estimates of the absorption coefficient.[23] Last, the analytical solution to the inverse OA

Address all correspondence to: A.A. Oraevsky, Fairway Technologies, Inc., 9431 West Sam Houston Pkwy. South, Houston, Texas 77099. Tel: 713-772-7867; Fax: 713-772-2010; E-mail: aoraevsky@fairwaymed.com

1083-3668/2009/14(2)/024007/14/$25.00 © 2009 SPIE

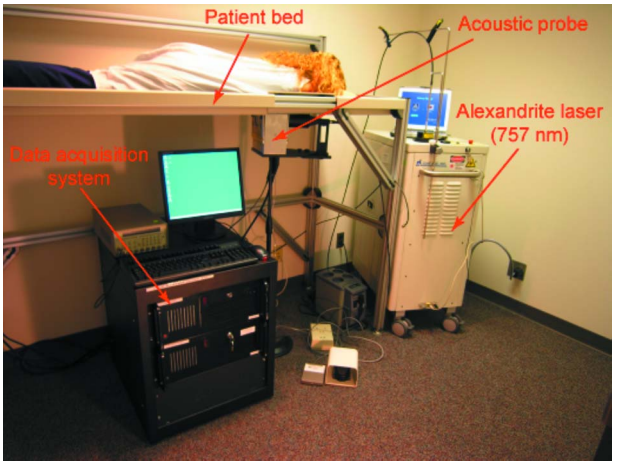

Fig. 1 LOIS-64 in a clinical setup.

problem has also been reported for the case when OA signals are known everywhere on an arbitrary surface enclosing the interrogated volume.[24–26]

Typical detected OA signals are the bipolar N-shaped pulses of wide-band ultrasound.[12] Therefore, OA transducers with the detection bandwidth from several tens of kHz to at least 2.5 MHz are required for appropriate imaging of objects with sizes between 1 mm and 20 mm (Ref. 27). In addition to such a wide bandwidth, the transducer sensitivity must be sufficiently high to permit detection of weak OA signals generated by the small objects located deep in tissue and illuminated with optical fluence not exceeding ANSI safety standards, i.e., $E_0 < 20$ mJ/cm^2 at the skin surface for NIR laser irradiation with low pulse repetition rate.[28]

This article reports the imaging characteristics of the laser optoacoustic imaging system (LOIS-64) for breast cancer detection. The system utilizes optical illumination in the NIR to maximize light penetration depth in the breast tissue while providing high absorption contrast of tumors. The ultrasonic detection within the ultrawide frequency bandwidth provides minimal distortions of measured OA signals and contributes to the high image resolution. The 2-D tomographic reconstruction of OA images of breast tissues is performed using the data collected in the orthogonal illumination mode with the cylindrical array of ultrasonic detectors.[11]

2 Materials and Methods

2.1 *System Description*

The LOIS clinical setup is shown in Fig. 1, and the corresponding schematic is shown in Fig. 2. The Q-switched Alexandrite laser (Ta2, Light Age, Inc., Somerset, New Jersey) was used as an NIR light source. The laser emitted 75-ns pulses (750 mJ/pulse) at 757 nm with the repetition rate of 10 Hz. The output laser beam was coupled into a custom-made optical fiber bundle and expanded with the lens system, producing a Gaussian profile on the surface of the breast. The laser beam incident on the surface of the breast was 70 mm in diameter and had a maximum fluence of 10 mJ/cm^2.

The acoustic detector probe (Fig. 3) represented a hemicylindrical cup in which the breast was suspended through the circular opening on the surface of the patient examination

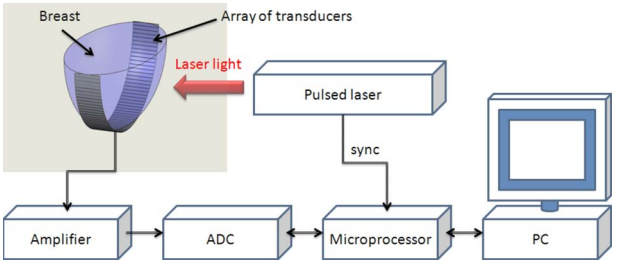

Fig. 2 Schematic diagram of LOIS-64.

table. The probe cup had the radius of its cylindrical surface of 70 mm and width of 90 mm, allowing accommodation of a large breast. The arc-shaped imaging array consisted of 64 rectangular polyvinylidene fluoride (PVDF a polymer piezoelectric material; Measurement Specialties, Inc., Hampton, Virginia) transducers ($20 \times 3 \times 0.11$ mm) and was used for reconstruction of 2-D images (mediolateral or craniocaudal), representing changes in optical absorption of the breast tissue within the imaging slice passing through the imaging array. The illumination with a wide laser beam orthogonally to the imaging array allowed small changes of optical fluence across the area of interest within the imaging slice, which was essential for good quality of the OA image.

The electrical signals generated by each transducer were amplified using a two-stage amplifier designed in house to respond to the wide bandwidth of the OA signals. The first stage, a charge amplifier, was designed for a low-noise amplification of microvolt signals generated by a capacitive source (OA transducer). The gain of this stage was 30 dB. Two of these preamplifier boards were used for the imaging array and were embedded in the acrylic body of the probe. The probe was covered with an electromagnetic (EM) shield to protect OA signals from any transmitted EM noise. The second stage, a standard 30-dB signal amplifier, was followed by an analog-to-digital converter (ADC) board based on 12-bit ADCs (AD9042, Analog Devices, Norwood, Massachusetts), which digitized the OA signals with a maximum sampling rate of 41 MHz. The data acquisition system communicated with a PC through the Ethernet interface and was controlled by a field-programmable gate array (Stratix II, Altera, San Jose, California). The LOIS-XP software allowed programmable control of the data acquisition (sampling rate and size of the data packets), system configuration (probe shape and size, the number of transducers, signal and image processing), and the

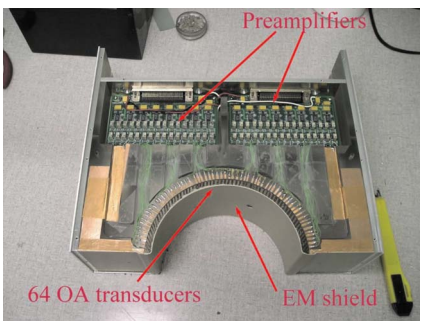

Fig. 3 Optoacoustic probe for LOIS-64.

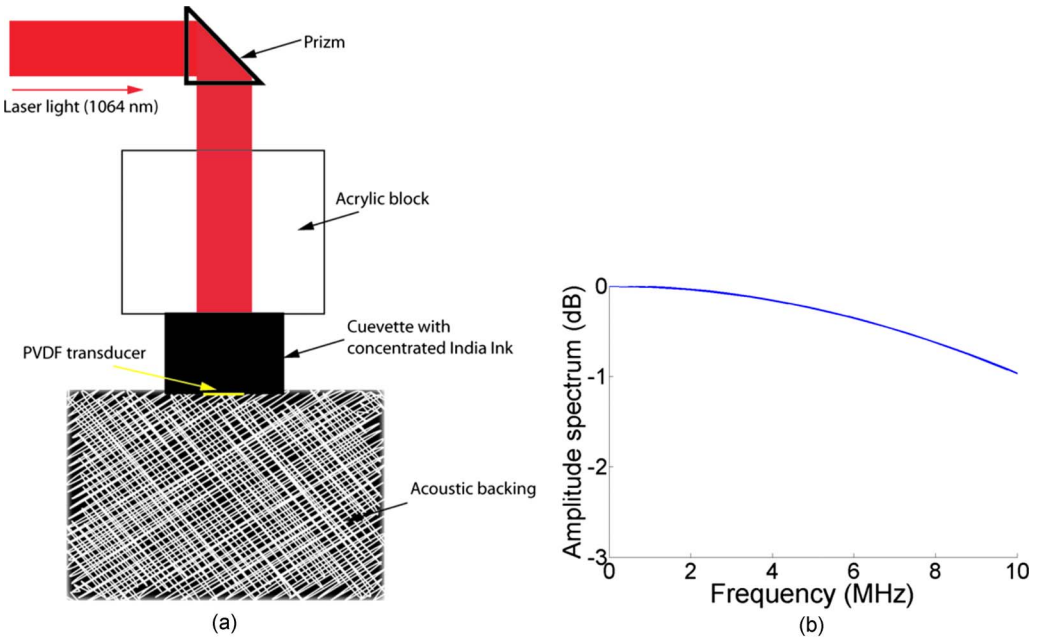

Fig. 4 (a) Setup for measurements of the transducer impulse response. (b) Amplitude spectrum of the acoustic signal generated during measurements of the transducer impulse response. Computer simulation.

real-time display of the signals from the individual transducers or the reconstructed images. The frame rate in the real-time imaging mode could be up to 1 frame per second for 512×512 pixel images and 10 frames per second for 128×128 pixel images.

2.2 *Measuring Impulse Response of an Acoustic Transducer*

Impulse response of a single acoustic transducer was measured as an electrical response to a planar acoustic wave generated by the 6-ns laser pulse absorbed in a layer of india ink (Sanford Higgins Fountain Pen india Ink, Sanford, Bellwood, Illinois). The laser light was emitted at the wavelength of 1064 nm by the Nd:YAG laser (Brilliant-B, Quantel, Bozeman, Montana). The concentrated india ink had an absorption coefficient $\mu_a \approx 1800\ \mathrm{cm}^{-1}$ at 1064 nm (extrapolated from the measurements on the diluted solution using a spectrophotometer—DU 520, Beckman Coulter, Fullerton, California). The schematic of the test setup is shown in the Fig. 4(a). The acrylic block (transparent for IR light) had an acoustic impedance about two times that of the india ink,[29] and it was used to create a hard acoustic boundary at the light-absorbing interface. The resultant short, monopolar, biexponential acoustic signal had essentially flat amplitude spectrum within the frequency band of interest [0 to 10 MHz; Fig. 4(b)], therefore representing the input δ-function. The acoustic signal was sensed by the PVDF transducer and recorded using an oscilloscope (TDS 3014, Tektronix, Beaverton, Oregon) with 10,000 samples at the sampling rate of 1 GHz.

2.3 *Measuring Sensitivity of a LOIS Channel*

The calibrated point acoustic emitter (NP/OA90-3, Dapco Industries, Ridgefield, Connecticut) was positioned in the imaging plane of the water-filled acoustic detector probe at a distance of 60 mm from the transducer array. A pivotal mechanism with a point of rotation located in the center of the probe was used to position the emitter over a specific transducer of the probe. The emitter was driven with a 20-cycle 1.5-MHz harmonic burst. The peak-to-peak driving voltage of 970 mV provided pressure amplitude of 85 Pa at the surface of the transducer.

2.4 *Directivity of an Acoustic Transducer*

The transducer sensitivity also depends on the incident angle of the acoustic wave and is described by the directivity of the transducer. For a finite-size transducer, the measured acoustic signal is a temporal convolution of the pressure signal at the transducer surface $p'(t)$ over the temporal transducer window function $T(\theta,t)$:

$$V_{tr}(\theta,t) = p'(t) * T(\theta,t) \cdot (k_n \sin\theta + k_\tau \cos\theta), \qquad (1)$$

where θ is the incident angle (angle between the acoustic wave vector and the surface of the transducer), $*$ indicates temporal convolution, and k_n and k_τ are the respective normal and shear acoustic sensitivities of the transducer. For the incidence plane (plane formed by the wave vector and the normal to the transducer surface) parallel to the side L of a rectangular transducer, the temporal transducer window function is:

$$T(\theta,t) = \frac{1}{a_T(\theta)} \Pi\left[\frac{t}{a_T(\theta)}\right], \qquad (2)$$

$$a_T(\theta) = \frac{L\cos\theta}{c_s}, \tag{3}$$

where Π is the rectangle function.

The signal received by a transducer at the right angle is not distorted and retains its amplitude. Therefore, the directivity function for a transducer $D_{\mathrm{tr}}(\theta)$ was defined as the ratio of the signal maximum at the incident angle θ to the signal maximum at $\theta=90$ deg. Using the temporal transducer window function (2), the directivity function for an incident N-shaped acoustic pulse generated by a spherical source[21,22] can be calculated as:

$$D_{tr}(\tau_p,\theta) = \left(\sin\theta + \frac{k_\tau}{k_n}\cos\theta\right)\begin{cases} 1-\dfrac{a_T(\theta)}{\tau_p}, a_T(\theta) < \dfrac{\tau_p}{2} \\ \dfrac{\tau_p}{4a_T(\theta)}, a_T(\theta) \geqslant \dfrac{\tau_p}{2} \end{cases}, \tag{4}$$

where τ_p is the N-pulse duration.

2.5 *Sensitivity of the Whole LOIS-64 System*

The sensitivity of the LOIS-64 system characterizes its capability to visualize small, weakly absorbing objects located in the imaging slice of the array of transducers.

As a simplified example, let us consider a spherical tumor. For this model tumor, the maximum magnitude of the temporal pressure integral (TPI) signal ($U_{\max}$) measured by a single transducer can be estimated as:

$$U_{\max}(d_0,z,r_{ct},\theta) = \frac{\Delta\mu_a \Gamma S E_0 d_0^2 D_{\mathrm{trI}}(d_0,\theta)}{16 c_s r_{ct}\exp(\mu_{\mathrm{eff}} z)}, \tag{5}$$

where d_0 is the diameter of the tumor, z is the distance between the imaging slice and the irradiated surface, r_{ct} is the distance from the center of the tumor to the transducer, $\Delta\mu_a$ is the differential optical absorption coefficient (tumor versus normal tissues), Γ is the Gruneisen coefficient[30] characterizing thermoelastic properties of the tumor, S is the sensitivity of the LOIS-64 channel within the signal bandwidth, μ_{eff} is the effective attenuation coefficient[31] of the breast tissue, and D_{trI} is the transducer directivity calculated for the TPI signal:

$$D_{\mathrm{trI}}(d_0,\theta) = \left(\sin\theta + \frac{k_\tau}{k_n}\cos\theta\right)\begin{cases} 1-\dfrac{a_T(\theta)^2}{3\tau_p^2}, a_T(\theta) < \tau_p \\ \dfrac{2\tau_p}{3a_T(\theta)}, a_T(\theta) \geqslant \tau_p \end{cases},$$

$$\tau_p = d_0/c_s. \tag{6}$$

We graphically visualized the total sensitivity of the LOIS-64 using the spatial distribution of the minimal tumor diameter $d_0^{\min}(\vec{r})$ detectable inside the imaging slice:

$$\sum_{i=1}^{N_{tr}} U^i_{\max}[d_0^{\min}, z_{tr}, r^i_{ct}(\vec{r}), \theta^i(\vec{r})] = \frac{N_{tr}}{\sqrt{N_{tr}-1}} U_{\mathrm{RMS}}, \tag{7}$$

where $\vec{r}$ is the spatial location inside the slice of an image, N_{tr} is the number of transducers in the imaging array, and U_{RMS} is the root-mean-square (RMS) noise of the TPI signal.

We assumed that a safe (clinically approved by ANSI) incident laser fluence ($E_0=20$ mJ/cm^2) is used during the optoacoustic imaging. We estimated the value of the Gruneisen coefficient for a breast tumor $\Gamma\approx 0.24$ using the following tissue material properties:[32] volumetric thermal expansivity $\alpha_p \approx 4\cdot 10^{-4}$ K^{-1}; speed of sound $c_s \approx 1500$ m/s; specific heat capacity $c_p \approx 3.7\cdot 10^3$ J/(kg·K). We estimated $\mu_{\mathrm{eff}} \approx 1.1$ cm^{-1} using the following optical properties of the breast tissue:[17] $\mu_s' = 9.5$ cm^{-1} and $\mu_a = 0.04$ cm^{-1}. We used the differential optical absorption coefficient for breast tumors relative to surrounding normal breast tissue $\Delta\mu_a \approx 0.05$ cm^{-1}.[17,18]

2.6 *Noise of the LOIS-64 System and the Signal Processing*

There are two types of noise, that affect the quality of the OA images obtained with LOIS: the first type is the electric noise, as represented by the external EM sources, and thermal fluctuations of the transducers and amplifiers.[27] The electric noise is reduced in LOIS by proper EM shielding and by limiting the high-frequency part of the amplifier bandwidth. The second type of noise comes from the OA sources, acoustic reflections, and probe resonance. Noise-generating OA sources are created by the optical energy absorbed within the skin and the first ~10 mm of breast tissue. They dramatically expand the dynamic range of the optoacoustic signals, thereby reducing the resolution and contrast of the image. Reflection of ultrasonic waves generated by strong OA sources from the acoustic boundaries, including echogenic areas inside the breast, physical breast boundaries, and the housing of piezoelectric transducers, also can be a source of acoustic noise. Last, an acoustically excited probe can resonate and create large low-frequency (LF) artifacts.

Acoustic reflections and signals generated by the probe were minimized in LOIS-64 by utilizing the probe material, which had proper acoustic matching to the breast tissue, and large acoustic attenuation. Narrowing the transducer directivity orthogonally to the imaging plane (see Sec. 3.2 helped to reduce OA signals generated on the illuminated surface of the breast and by other OA sources located outside the imaging plane.[33]

An important feature of the optoacoustic signal used for the designing of an optimal signal processing was the bipolar shape (N-shape) of the measured pressure pulses with a very short rise time and, simultaneously, significant energy residing in the low-frequency band (below 1 MHz).[27] Additionally, the visualized breast tumors could be anywhere between 5 mm and 20 mm in size, generating N-shaped pressure pulses with different spectral bands. Therefore, in order to eliminate-LF acoustic artifacts and simultaneously transform the bipolar pressure pulse to the monopolar pulse suitable for the tomographic reconstruction of the OA image, we implemented the wavelet transform using a wavelet family resembling the N-shaped OA signal.[34] The wavelet transform has been estab-

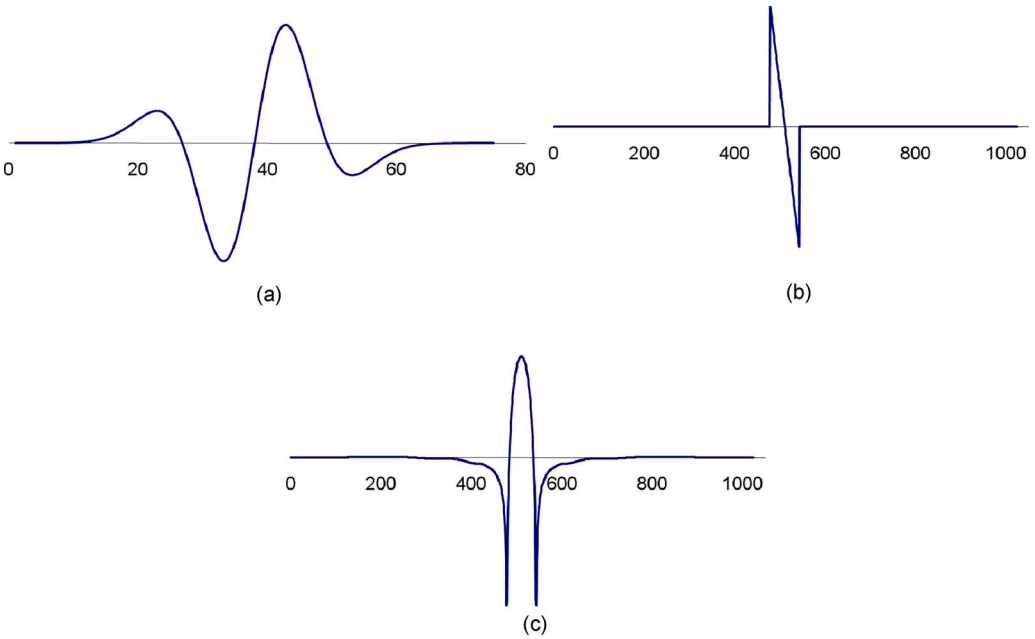

Fig. 5 (a) Third derivative of the Gaussian wavelet. (b) N-shaped OA pressure signal. (c) OA pressure signal transformed with nine scales of the wavelet.

lished in signal processing as a superior tool for pattern recognition and temporal localization of specified signal patterns.[35] We found that the third derivative of the Gaussian wavelet [Fig. 5(a)] was the best candidate for filtering the N-shaped signals [Fig. 5(b)], providing a monopolar pulse with enhanced sharpness of the boundaries [Fig. 5(c)], while significantly reducing LF acoustic artifacts [Fig. 13(d)].[36] In the frequency domain, the chosen wavelet had a narrow bandpass region and a steep slope in the LF band, which allowed more precise recovery of the OA signals by using a large number of wavelet scales (up to nine scales, with filter lengths ranging from 4 to 1024 data samples).

2.7 *Reconstruction of OA Images*

To reconstruct a 2-D OA image from pressure signals measured by the imaging array, we used the radial back-projection algorithm.[11,24] Briefly, the algorithm employs temporal integration of the pressure signals. Then each sample s of the digitized TPI is added to the corresponding pixels of the image located on the intersection of the imaging plane with spherical surface of radius $R=c_s\Delta t(s-1)$, where Δt is the sampling period. Additionally the algorithm weighs the values according to the directivity diagram of each transducer (see Sec. 2.4).

2.8 *Computer Simulation of the Optical Energy Absorbed by the Breast Tissue*

Three-dimensional distribution of the optical properties (index of refraction, absorption coefficient, scattering coefficient, and scattering anisotropy) simulating breast tissues inside the acoustic detector probe was the core of the model based on the Monte Carlo method.[37] The modeling was used to generate 3-D distribution of the optical energy absorbed within the breast tissue. Table 1 contains the values of the optical parameters used, and Fig. 6 explains the structural features of the model. The modeling was performed using 10 million photons for the 70-mm-diam Gaussian laser beam. The beam was incident orthogonally to the skin at $x=0$ mm and $y=-35$ mm from the center of the probe.

2.9 *Phantoms Used in Studies of the OA Image Contrast and Resolution*

We used a phantom based on the aqueous milk solution representing a female breast with a tumor to study the acoustic artifacts and the contrast of OA images. The aqueous milk solution was chosen because it had acoustic properties close to those of the breast tissue and was easy to prepare with desired optical properties. The required optical absorption coefficient was achieved by the dissolved india ink. The optical properties of the liquid phantoms used in experiments were measured with an integrating sphere (RT-6, SphereOptics, Concord, New Hampshire). We filled the LOIS-64 probe with solution having optical absorption coefficient $\mu_a=0.04$ cm^{-1} and reduced scattering coefficient $\mu_s'=9$ cm^{-1}. For studies of the image contrast and OA artifacts, we positioned a thin-wall rubber shell (10 mm in diameter, 10-μm wall) filled with the

Table 1 Optical properties of the breast used in modeling of absorbed optical energy (Refs. 17 and 31).

Tissue	Index of refraction	Absorption coefficient (cm^{-1})	Scattering coefficient (cm^{-1})	Scattering anisotropy
Skin	1.4	0.2	75	0.8
Normal breast	1.4	0.04	100	0.9
Tumor	1.4	0.1	120	0.9

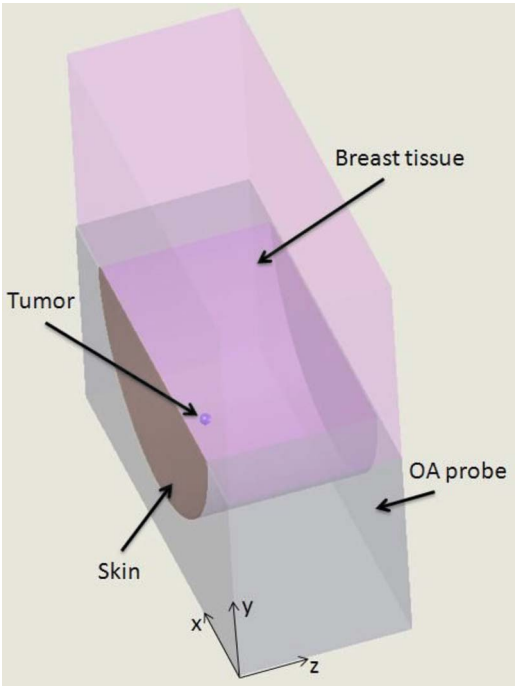

Fig. 6 Schematic of the model used to simulate the distribution of the optical energy absorbed by the breast tissue during optoacoustic imaging with LOIS-64. Skin layer was 1 mm thick. Tumor was 5 mm in diameter and located $z=20$ mm from the skin; $x=-10$ mm and $y=-30$ mm from the center of the OA probe

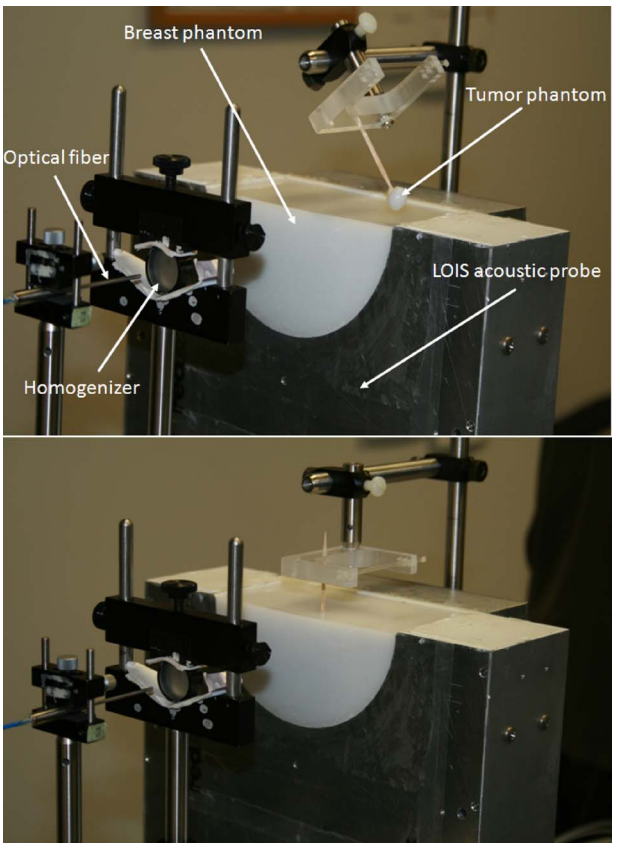

Fig. 7 Experimental setup for studies of the OA image contrast.

solution mimicking the tumor ($\mu_a=0.15$ cm^{-1}, $\mu_s'=12$ cm^{-1}) inside the imaging slice of the probe about 20 mm below the illuminated surface (Fig. 7). For studies of the image resolution, we positioned two parallel plastic tubes (inside diameter 0.7 mm, wall thickness 0.05 mm; Zeus, Orangeburg, South Carolina) filled with the india ink dissolved in an aqueous milk solution ($\mu_a=2.8$ cm^{-1}, $\mu_s'=4$ cm^{-1}) inside the imaging slice of the probe [Fig. 8(a)]. The ink-filled interiors of the tubes were separated by 0.5 mm [Fig. 8(b)]. The incident laser fluence was 1.4 mJ/cm^2.

2.10 *Preliminary Clinical Studies on Breast Cancer Patients*

Preliminary clinical studies of the LOIS-64 were held in the Radiology Department at the University of Texas Medical Branch (Galveston, Texas) under institutional review board (IRB) Protocol #99464. A total of 42 patients participated in the studies. In the first phase, the safety studies were performed on 15 patients scheduled for radical mastectomy. The pathology studies performed on breasts surgically excised after LOIS imaging demonstrated safety of laser illumination and absence of thermomechanical damage to tissues.[10] In the second phase, a patient with a suspicious breast region identified on the mammography and/or ultrasonic image was scheduled for breast biopsy. Prior to the biopsy, an imaging with LOIS was performed. The recorded OA signals were processed with the 8-scale wavelet transform and used in the reconstruction of the OA image according to the procedure described in the Sec. 2.7. The linear grayscale palette of the resultant OA image was individually optimized in each case to get the maximum image contrast. The OA images were visually analyzed and compared to the mammography and ultrasonic images. We considered that the tumor can be seen on the OA image if an isolated area of increased intensity could be localized in the quadrant of the breast suspected to contain a tumor according to the ultrasound and mammography images. The final diagnosis was made based on the biopsy results.

During the second phase, the LOIS prototype hardware, software, and imaging procedure were continuously optimized for the best performance, with the latest design presented in this work. The details on the technical parameters and performance of some intermediate versions of LOIS can be found in our previous publications.[10,11,23,38] Due to system modifications, no statistical inferences could be made during the second phase of the preliminary clinical studies. In this work, we report the capability of LOIS to visualize breast cancer based on the 27 cases studied during the second phase of the preliminary clinical studies. Two cases that demonstrate the feasibility of clinical application of the LOIS-64 are discussed in greater detail.

3 Results

3.1 *LOIS Frequency Response*

Using the technique described in Sec. 2.2, we measured the impulse response of an individual acoustic transducer [Fig. 9(a)]. Acoustic backing of PVDF transducers was provided by an acoustically matching scattering and absorbing composite,

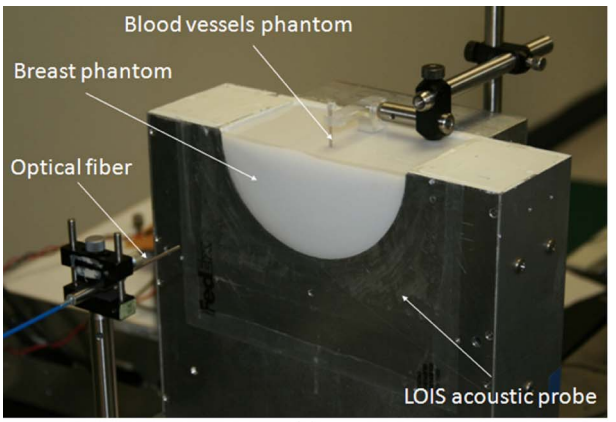

(a)

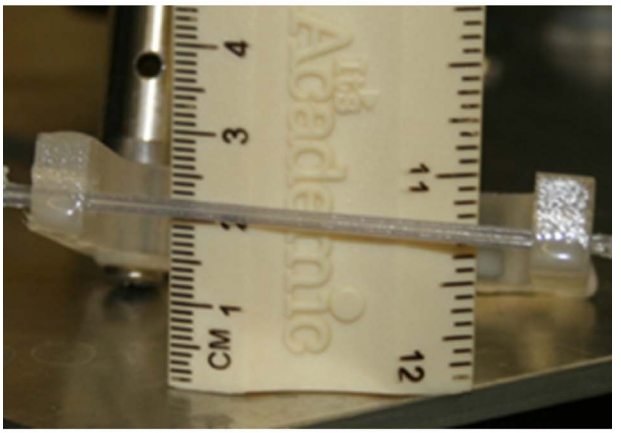

(b)

Fig. 8 (a) Experimental setup for studies of the OA image resolution. (b) Two parallel plastic tubes filled with the india ink solution separated by 0.5 mm used to simulate blood vessels.

which caused no reverberations after detection of a pressure pulse [Fig. 9(a)]. The frequency response of PVDF transducers is shown in the Fig. 9(b), having a bandwidth up to 2.5 MHz. Because both amplification stages were operated in the wideband mode, the system frequency response followed that of the PVDF transducer.

3.2 *Sensitivity of an Individual LOIS Channel and the Whole LOIS-64 System*

Using the methodology described in Sec. 2.5, we measured the average sensitivity of an individual LOIS channel to a

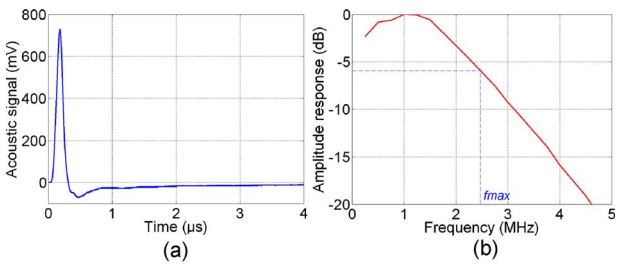

Fig. 9 (a) Impulse response of a PVDF transducer used in LOIS-64. (b) The corresponding amplitude response ($f_{max} \approx 2.5$ MHz).

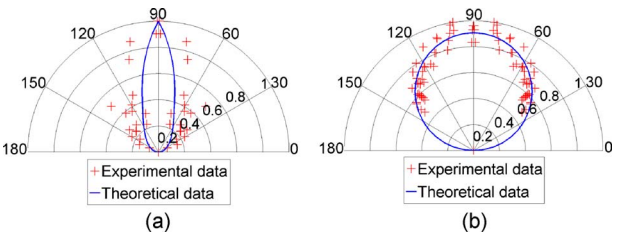

Fig. 10 Directivity of individual transducers used in LOIS-64. OA target is a 9.5-mm polyvinyl chloride–plastisol ball. Graphs made in the polar coordinate system show the amplitude of the measured OA signal as a function of the incident angle (deg). The data is normalized to the amplitude of the OA signal measured for orthogonally incident acoustic wave. (a) Directivity in the plane parallel to the long side of the transducer (20 mm); (b) directivity in the imaging plane.

normally incident 1.5-MHz acoustic wave to be 1.66 mV/Pa, with a standard deviation of 0.21 mV/Pa (N=46). The sensitivity of an individual LOIS channel to normally incident acoustic waves at other frequencies could be derived from the transducer frequency response shown in the Fig. 9(b).

For the N-shaped pressure wave incident parallel to the long side of the planar rectangular transducer, the convolution (1) leads to a narrow directivity [±15 deg, based on the −6-dB level; see Fig. 10(a)]. Our experimental data (crosses) confirmed that the LOIS-64 produces 2-D images of slices with a thickness of about the length of the long side of the transducers (20 mm). On the other hand, the short side of LOIS transducers (3 mm) provides directivity close to ±60 deg within the imaging slice [Fig. 10(b)].

The measured RMS noise of the TPI signal was $0.22 \cdot 10^{-7}$ V·s. Using Eq. (7), we calculated that for a single-pulse data acquisition. a tumor with diameter of 6 to 11 mm could be detected by LOIS-64 through the entire imaging slice (Fig. 11).

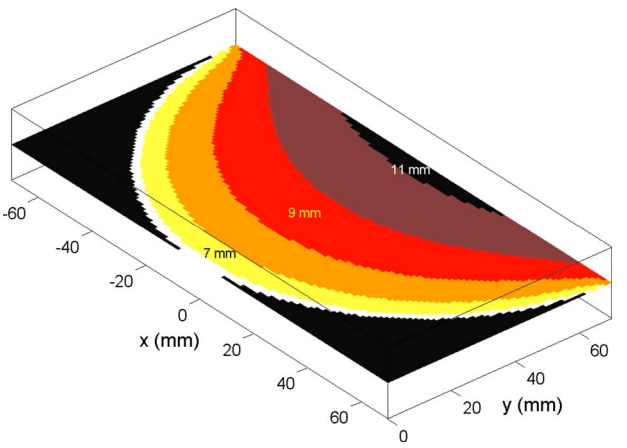

Fig. 11 Minimal diameter of a tumor detectable by LOIS-64 in the imaging slice. Signal-to-noise ratio is 1; single-pulse acquisition. Computer simulation. Minimal diameters of detectable tumors are linearly scaled on the image palette from 6 mm to 11 mm. Area within the imaging slice painted with a particular color specifies possible locations of the center of the tumor, which would be detected by the array, providing its diameter is greater than or equal to the one coded by that color. (Color online only.)

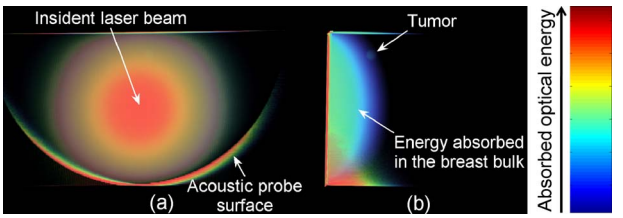

Fig. 12 Monte Carlo simulation of the optical energy absorbed by the breast within the LOIS-64 probe. (a) Front view, showing Gaussian transverse profile of the laser energy absorbed within the breast and the energy absorbed by the surface of the acoustic probe. (b) Side view, showing distribution of the laser energy absorbed by the breast tissues along the direction of light propagation as well as the tumor.

3.3 *OA Artifacts, Signal Processing, and Image Contrast*

Figure 12 displays the Monte Carlo simulation of 3-D distribution of the optical energy absorbed by the breast within the LOIS-64 probe, illustrating the nature of LF acoustic artifacts. The large volume in the front part of the breast where laser light enters the tissue contains a significant amount of the absorbed optical energy. Also part of the probe's surface is receiving some light, which creates strong OA signals. Both of those phenomena resulted in large-magnitude LF OA signals that dominated the much smaller N-shaped pulse generated by the 5-mm spherical tumor located in the imaging slice just 20 mm below the skin [Fig. 13(a)]. The corresponding TPI signals [Fig. 13(b)], used for the image reconstruction, provided low-pass filtering, therefore enhancing the LF artifacts and resulting in a very poor contrast of the reconstructed OA image [Fig. 14(a)]. Figure 13(c) displays the signal, and Fig. 14(b) displays the image obtained by filtering with the optimized 75-kHz finite impulse response (FIR) high-pass filter with the Hamming window followed by the integration. Despite the removed LF artifacts, the subsequent integration significantly reduced the rise time of the signal and the sharpness of the OA image. Application of the 8-scaled wavelet transform made the tumor signal clearly visible [Fig. 13(d)], and significantly improved the tumor contrast on the reconstructed OA image [Fig. 14(c)]. Using fewer scales in the wavelet transform highlighted fast-changing signals from the boundaries of the tumor and flattened the background even more [Figs. 13(e) and 14(d)]. However, the contrast of the tumor interior disappeared [Fig. 14(d)]. A very low signal-to-noise ratio(SNR) can be observed when a post-processing differentiation is used in the attempt to enhance high-frequency features of the OA signals [Fig. 13(f)], as is done in some algorithms used in the OAT.[39] The differentiation results in a poor contrast of the image but enhances boundaries of the object in a way similar to the low-scaled wavelet transform [Fig. 14(e)]. Also, in this case, the image contrast could be improved if differentiation of the pressure signals is done by the hardware. The effect of averaging on the tumor contrast was demonstrated in Fig. 14(c) (256 averaged acquisitions) versus Fig. 14(f) (no averaging). The arc-shaped artifacts seen around the tumor phantom are caused by the powerful OA signal generated at the air–fluid interface and reflected from the phantom target toward the transducers. When reconstructed using a regular radial back-projection technique, such

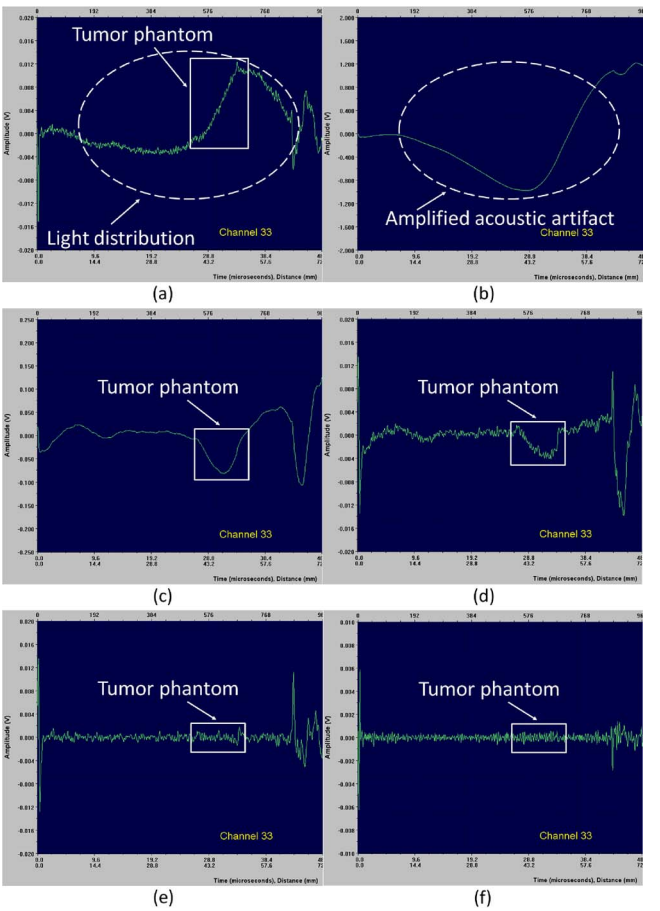

Fig. 13 Processing of the OA signals from the tumor phantom. (a) Original signal showing the small N-shaped pulse riding on the large LF acoustic artifact. (b) Integration of the measured pressure wave form showing amplification of the LF acoustic artifacts. (c) Application of the 75-kHz FIR high-pass filter with Hamming window followed by the integration. (d) Eight-scaled transform using the third derivative of the Gaussian wavelet; retains the short rise time of the tumor signal. (e) Six-scaled transform using the third derivative of the Gaussian wavelet; highlights the edges of the tumor signal. (f) Differentiation of the measured pressure wave form; reduces signal-to-noise ratio.

signals will produce a distorted image of the target. The artifacts still persist after the applied signal processing [Figs. 14(b)–14(f)].

3.4 *Resolution of the OA Images*

Figure 15 displays OA images obtained with the resolution phantom using high-pass filtering and wavelet-based signal processing. Using the optimized high-pass filter with a cutoff frequency around 400 kHz allowed resolution of 0.5 mm with horizontal orientation of the tubes [Fig. 15(a)]. However, the image contrast was very poor in comparison to the results obtained with the 6-scaled wavelet transform [Fig. 15(b)]. The high-pass filtering of OA signals followed by integration was unable to resolve 0.5 mm with a vertical orientation of the tubes [Fig. 15(c)], while the 5-scaled wavelet provided clear high-contrast images of the separate tubes [Fig. 15(d)]. The arc-shaped artifacts, created by the acoustic waves reflected from the resolution phantom, and described in the previous

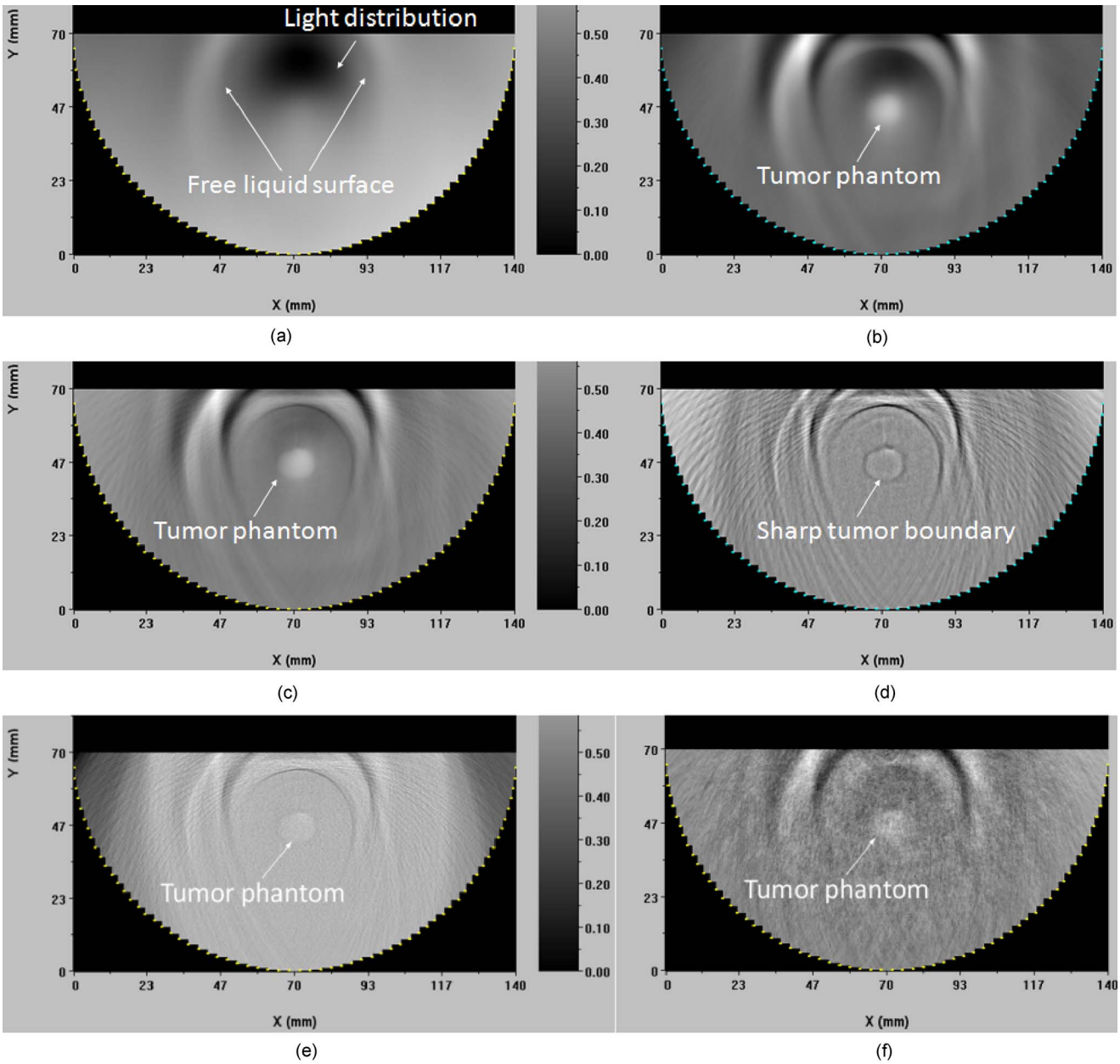

Fig. 14 OA images of the tumor phantom. (a) RBP with the integration of the measured pressure wave form. (b) Application of the 75-kHz FIR high-pass filter with Hamming window followed by the integration, showing high tumor contrast but significant blurring. (c) 8-scale transform using the third derivative of the Gaussian wavelet; retains the high contrast and minimizes blurring of the tumor. (d) Six-scaled transform using the third derivative of the Gaussian wavelet; highlights the tumor boundaries. (e) RBP using the differentiated pressure wave form; provides sharp images but with low contrast. (a) to (e) Acquisition with 256 averaged laser pulses. (f) Eight-scaled transform using the third derivative of the Gaussian wavelet. Acquisition without averaging.

section, are particularly apparent on the images with vertical orientation of the tubes [Figs. 15(c) and 15(d)].

3.5 *Demonstration of the Clinical Performance of the LOIS-64*

In the clinical study on 27 patients using LOIS-64, biopsy performed after LOIS procedure revealed 34 lesions, including 26 malignant tumors (25 carcinomas and 1 papilloma with focal area of rapid abnormal cell growth) and 8 benign formations (3 fibroadenomas, 3 fibrocystic lesions, and 2 regions of fibrosis with calcifications). In one dense breast suspected to contain a tumor based on the x-ray mammography, the ultrasound did not find any abnormalities, and biopsy was not performed. The OA images identified (see Sec. 2.10 for details on the visualization criterion) 22 lesions, including 17 carcinomas, 1 papilloma with focal area of rapid abnormal cell growth, 2 fibroadenomas, 1 fibrocystic lesion, and 1 region of fibrosis with calcifications. Of the eight cases when OA imaging failed to identify the cancer, in two cases, the OA image was reconstructed but the tumor could not be visualized due to insufficient contrast, five cases were due to the system malfunction, and one case was due to operator error.

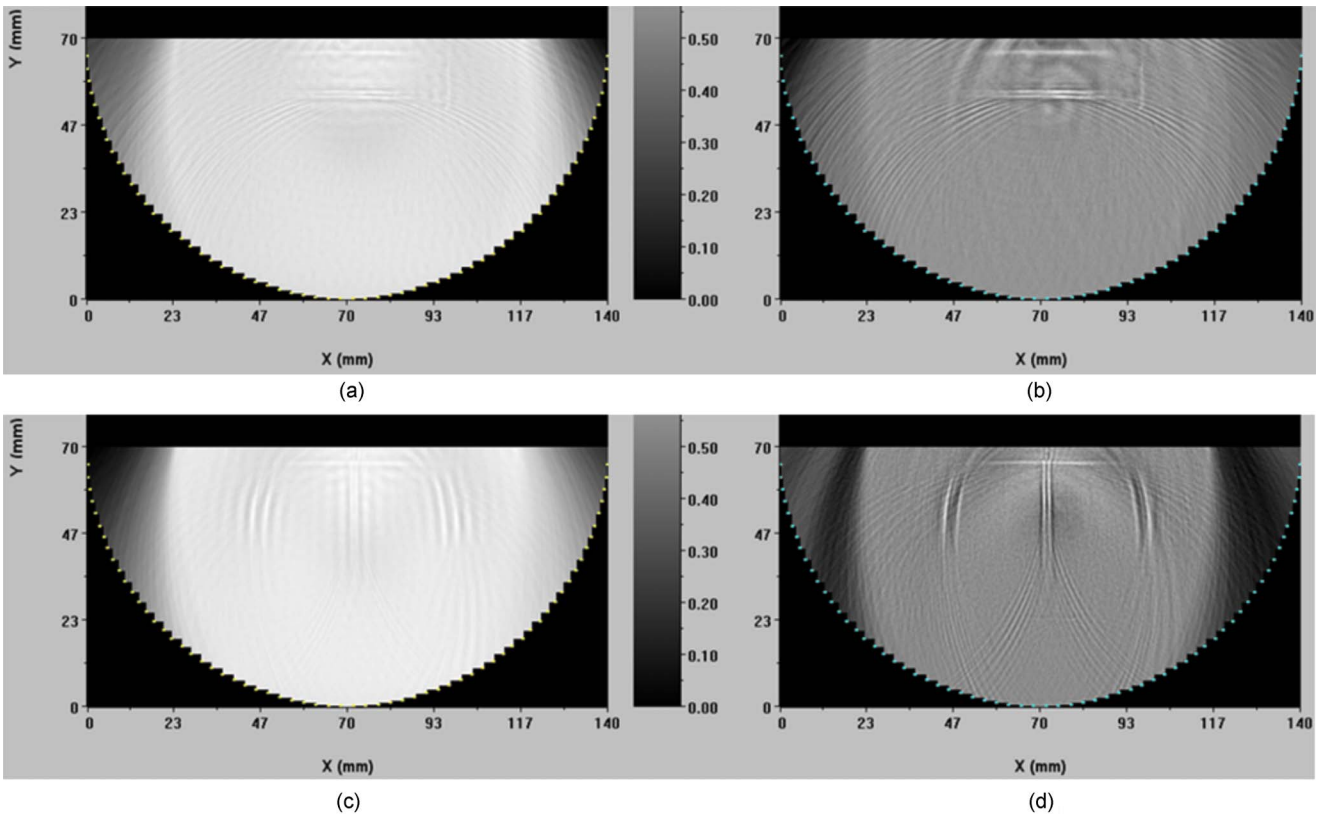

Fig. 15 OA images of the resolution phantom. Application of the 400-kHz FIR high-pass filter with Hamming window optimized for high-resolution imaging followed by the integration; provides 0.5-mm horizontal resolution (a) but very poor contrast and worse than 0.5-mm vertical resolution (c). Application of the 6-scaled (b) and 5-scaled (d) transform using the third derivative of the Gaussian wavelet; provides 0.5-mm horizontal and vertical resolution and high image contrast.

Table 2 summarizes the efficiency of a breast tumor visualization using ultrasound, mammography, and OA imaging. The studied malignant tumors were between 11 and 26 mm in size, with the centers located 8 to 26 mm inside the breast.

An example of how LOIS-64 can improve x-ray mammography is depicted in Fig. 16. The tumor (poorly differentiated infiltrating ductal carcinoma grade 3/3, according to the biopsy) could barely be localized on the mammography image of the radiologically dense breast [Fig. 16(a)]. The auxiliary ultrasonic imaging helped to identify a 23×15 mm tumor located at the depth of 21 mm [Fig. 16(b)]; however, the tumor margins were not clear. The tumor was clearly seen on the OA image [Fig. 16(c)] at the same location as determined by the ultrasound and mammography. The tumor contrast on the OA image exceeded the tumor contrast on the ultrasonic image (judged by the visual comparison of the images created using the same linear grayscale palette) and was attributed to the associated microvasculature.

Table 2 Summary of the preliminary clinical studies using LOIS.

Visualized with	Number of malignant breast tumors
Either mammography, ultrasound, or LOIS (not considering cases of technical problems during OA imaging)	20
Mammography	14
Ultrasound	20
LOIS	18
Mammography but not LOIS	1
LOIS but not mammography	5
Neigher mammography nor LOIS	1

In another case, the mammography image in Fig. 17(a) revealed the round shape of the tumor (about 15 mm in diameter located 16 mm under the skin), suggesting that it was benign. However, the LOIS image [Fig. 17(c)] exposed a focal area of enhanced brightness indicative of the advanced angiogenesis. The additional imaging with the color Doppler ultrasound [Fig. 17(b)], confirmed enhanced blood flow in one focal area of the tumor. The biopsy of this tumor revealed the intraductal papilloma with some clusters of rapidly growing cells of unusual (abnormal) pathology, indicating possible malignancy.

4 Discussion

The measured impulse response of LOIS-64 allows us to predict the accuracy of the measured OA signals and maximum

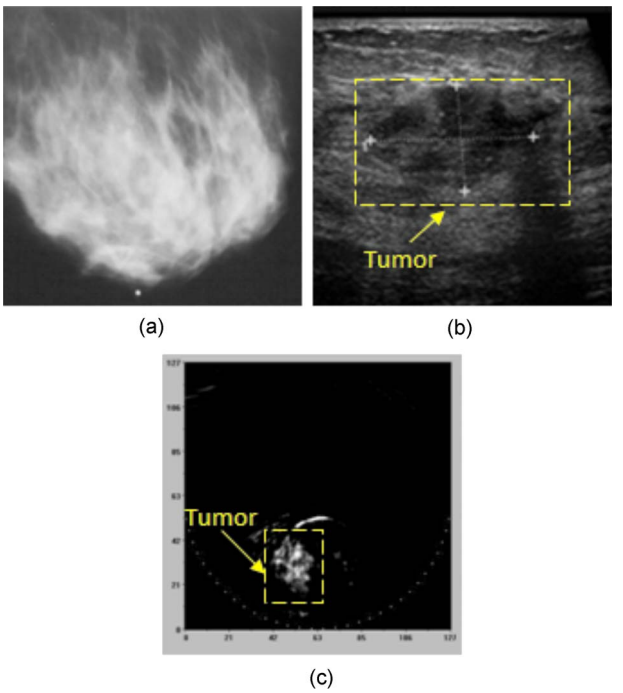

Fig. 16 Example of the clinical images showing the breast cancer: (a) mediolateral mammography, (b) ultrasonic, and (c) mediolateral optoacoustic images. High contrast of the object in the OA image implies the advanced angiogenesis indicative of a malignant tumor.

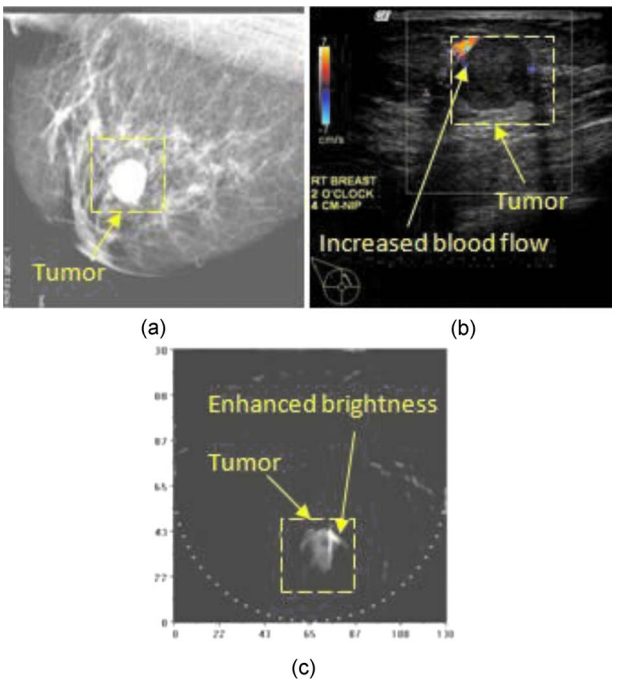

Fig. 17 (a) Digital mammography image (mediolateral projection) of the breast, showing a round, apparently benign tumor. (b) Ultrasonic imaging with the Doppler showing the tumor boundaries and the focal blood flow increase. (c) Optoacoustic image (mediolateral projection) showing the enhanced contrast around the area of the focal blood flow increase detected by the Doppler ultrasound.

resolution of the system. Convolving the N-shaped OA signal [Fig. 5(b)] with the impulse response [Fig. 9(a)] results in less than 10% amplitude distortion in signals with temporal width above 1.4 μs, corresponding to a 2-mm spherical object. Accurate measurements of the OA signal amplitude are necessary to reconstruct the local absorption coefficient measured at different wavelengths, which could be used later in quantitative analysis of the major breast tissue chromophores: oxyhemoglobin, hemoglobin, water, and lipids. A similar approach was implemented in the diffuse optical spectroscopy[17,18,40] to enhance the diagnostic power of the technique.

The wideband transducers utilized in LOIS-64 reproduced OA signals without ringing, and their maximum spatial resolution can be determined from the width at half magnitude ($\tau_{0.5}$) of the transducer impulse response [Fig. 9(a)]:

$$\delta_{\min} \approx c_s \tau_{0.5}. \tag{8}$$

From that criterion, the maximum spatial resolution of a single LOIS-64 transducer was estimated as $\delta_{\min} \approx 165$ μm. In the current studies, we were unable to investigate the resolution of OA images less than 0.5 mm. However, the two sets of clinical images (Figs. 16 and 17) revealed the challenges in resolving the dense abnormal microvascular network, which is considered to be a marker that the lesion has passed its dormant stage and is expanding to tumor mass.[41,42] This problem can be approached by studying the resolution limits of LOIS-64 using multiple randomly oriented high-aspect-ratio objects.

The sensitivity of LOIS-64 reported in the Sec. 3.2 was estimated for a single laser pulse acquisition considering only the random component of the noise. However, during clinical imaging or imaging of the realistic breast phantoms, the noise level is set by the acoustic artifacts, described in detail in the Sec. 3.3. That type of noise is not random and cannot be diminished through averaging. Moreover, both the acoustic noise and the OA signals from the tumors increase proportionally to the fluence of the incident laser beam, producing virtually identical images, while laser fluencies differ several times. The only way to improve the sensitivity in the presence of such noise is to apply proper signal processing. We showed that the designed wavelet transform is capable of bringing the level of the direct acoustic noise (a component of the acoustic noise caused by the direct detection of the acoustic signals generated by the light distribution within the bulk tissue) below the level of the random noise [see the significant improvement after averaging signals 256 times—Fig. 14(c) in comparison to Fig. 14(f)] allowing manipulation of the SNR through averaging and adjustments in the incident laser fluence. However, the reflected acoustic noise (see Secs. 3.3 and 3.4) is invincible to the applied signal processing. Currently, we investigate the possibility of deconvolving the direct and reflected acoustic noise from the OA image by taking advantage of the known characteristics of the acoustic sources causing those acoustic artifacts.

An example that testifies for a high sensitivity of the LOIS-64 is that with incident optical fluence of just 1.4 mJ/cm^2 we could clearly visualize a 14-mm sphere with $\Delta\mu_a = 0.03$ cm^{-1} located inside the scattering medium ($\mu_s' = 12$ cm^{-1}) at a depth of 20 mm from the laser-illuminated surface and 50 mm from the ultrasonic detectors. The sensitivity of LOIS is sufficient for OA detection of breast cancer

based on endogenous contrast of blood in the angiogenesis-related tumor microvasculature, and it can be further increased by using delivery of cancer-specific optical contrast agents.[43–45]

In this work, we estimated the directivity of individual LOIS-64 transducers based on the theoretical N-shaped OA signals generated by a spherical source,[21,22] (see Secs. 2.4 and 3.2). However, in reality, the tumor shape may significantly deviate from a sphere. In that case, the transducer spatial impulse response[46] is the only way to correctly describe the sensitivity of a transducer to OA sources located at different spatial positions. The approach requires complex experimental equipment (point acoustic delta-source) to measure the spatial impulse response of a transducer and much more computational power (memory and processing speed). Nevertheless, we anticipate that the spatial impulse response approach will ultimately be used in OAT as soon as the related technical issues are solved.

Knowledge of the light fluence distribution within the breast tissue is required for the quantification of the local absorption coefficient. The LOIS-64 system was designed only for visualization of breast cancer and does not employ any quantitative image characteristics for diagnostic purposes. However, for the best quality OA image, representing changes in the optical absorption of the tissue, the light fluence should not significantly change across the area of interest within the imaging plane. In other words, it is desirable to have homogeneous light distribution orthogonally to the direction of light propagation. In LOIS-64, we implemented the terminal optical system allowing wide-beam (about 70 mm in diameter) illumination of the breast surface. Using the Monte Carlo light-distribution model (see Sec. 2.8), we estimated that about 20% of the imaging slice around the center of the laser beam had deviations of the light fluence less than 25%. Therefore, if accurate quantitative information has to be obtained from the whole imaging slice, the beam must be either scanned or further expanded.

Another distinctive feature of the LOIS technology is fast imaging. In the current version of LOIS-64, the image refresh rate is defined primarily by the time it takes for a computer to reconstruct a 2-D map of image pixels. All other operations, such as signal processing and data transmission to the computer are performed much faster than the image reconstruction. We achieved a frame display rate of 1 Hz for 512 $\times$512 pixel maps using a standard PC with a single 3-MHz processor. Utilization of the multithreaded parallel computation with a computer having four processors resulted in a real-time OA imaging with a frame rate of 10 Hz for 256 $\times$256 pixel images.

Our preliminary clinical studies demonstrated the feasibility of using LOIS as a high-contrast modality for imaging of breast cancer. Disregarding the cases when OA images could not be obtained due to technical reasons, LOIS was able to visualize 18 malignant tumors out of 20 detected by biopsy (see Table 2). Among those 18 visualized tumors, 5 were not seen on mammography images, while only 1 tumor was seen on the mammography image and not visualized by LOIS. The fact that all 20 malignant tumors were seen on the ultrasonic images was consistent with reported high sensitivity of ultrasound breast cancer imaging (sometimes more than 99%).[1,47] However, ultrasound breast cancer imaging is not used nowadays as a stand-alone technology for a variety of reasons, including high false-positive rates and operator dependence.[1] Considering that ultrasound and OA imaging technologies are based on very similar principles and engineering solutions, it would be logical to utilize them in a hybrid modality with enhanced diagnostic capabilities for breast cancer (especially in cases of radiologically dense breasts, when mammography is considered ineffective). In the hybrid ultrasound-OA imaging system, ultrasound imaging would provide information about acoustic boundaries, while OA imaging would map the vascular distribution in the vicinity of a tumor. The methodology used in these studies for OA visualization of breast tumors (see Sec. 2.10) was designed to get preliminary estimates regarding the sensitivity of LOIS for breast cancer detection. After the system parameters are fixed, sufficient clinical statistics on different types of breast tumors must be accumulated in order to determine the actual sensitivity and specificity of OA breast cancer imaging as a stand-alone application and as a part of the hybrid modality (with ultrasound and/or mammography).

The LOIS-64 system can visualize only a single breast slice—the imaging slice. In order to see a large volume of the breast, several acquisitions have to be taken while the OA probe and the laser beam are rotated about the breast axis of symmetry. This is rather cumbersome and it takes a significant amount of time to reposition the breast. Considering the origin and propagation of the OA signals,[24,48] it is reasonable to assume that a 3-D OAT system would outperform LOIS-64 in terms of the speed of 3-D image reconstruction. However, there are some fundamental problems related to the image quality obtained with a 3-D OA system that impede its development. In spite of the advantages in resolution brought about by the large acoustic aperture of a 3-D OA system, the major problem comes from the light distribution within the breast tissue, with the fluence changing about an order of magnitude over a 2-cm distance. Simultaneously, the expected average tumor absorption contrast over the background is just about 2:1 (Ref. 17). Assuming also that a typical 1-cm tumor is located 2 cm under the skin surface, we estimate that its meridianal section is equal to about 3% of the TPI-forming portion of the sphere (see Sec. 2.7). Therefore, only about 0.5% of the TPI signal will contain the information about the tumor. The rest will be contribution from the acoustic noise. There are of course additional problems associated with the processing power requirements for the 3-D OAT system. Nevertheless, we strongly believe that future improvements in light illumination, manufacturing of 2-D transducer arrays (OA probes), and data processing would allow an OAT system built on the 3-D technology to become a useful addition to the arsenal of the imaging modalities used by the breast radiologist.

5 Conclusion

A laser optoacoustic imaging system (LOIS) was developed and characterized in terms of its frequency-dependent acoustic sensitivity and spatial resolution. The computer simulations and experiments in breast phantoms were used to analyze OA signals and images and determine optimal methods for signal processing. This in turn allowed us to visualize phantom tumors with low physiologically relevant values of

optical absorption contrast of $\sim 0.03\ cm^{-1}$ in the presence of optically absorbing and scattering background resembling the properties of breast tissue. Spatial resolution of LOIS determined in the optically scattering medium was ~0.5 mm. This study demonstrated that considerable challenges presented by the low-frequency acoustic artifacts (reflection and reverberations within the breast and the detecting probe) and limited directivity of the transducer array can be overcome, encouraging development of future commercial generations of LOIS for applications in diagnostic imaging.

Pilot clinical studies in 27 patients performed using the developed system demonstrated the high contrast of OA images of breast tumors, which takes advantage of the blood optical absorption in the angiogenesis-related microvasculature. We suggest that the developed clinical optoacoustic system can be utilized as a dual ultrasonic/optoacoustic real-time imaging modality providing functional information directly correlated with morphological information of the breast ultrasound.

Acknowledgments

This work was supported in part by grants from the National Cancer Institute (R44CA110137, R44CA128196, R33CA095883, and R44CA089959), the U.S. Army Breast Cancer Imaging Research Program (W81XWH-04-1-0484), and Seno Medical Instruments, Inc. (San Antonio, Texas).

We thank the technical staff of Fairway Medical Technologies for their contributions to LOIS engineering and assembly. We also thank Wenjeng Li and Jack Fuqua for their help in the preparation of this manuscript.

References

1. J. A. Smith and E. Andreopoulou, "An overview of the status of imaging screening technology for breast cancer," *Ann. Oncol.* **15**(Suppl 1), I18–I26 (2004).
2. U. Veronesi, P. Boyle, A. Goldhirsch, R. Orecchia, and G. Viale, "Breast cancer," *Lancet* **365**(9472), 1727–1741 (2005).
3. L. Irwig, N. Houssami, and C. van Vliet, "New technologies in screening for breast cancer: a systematic review of their accuracy," *Br. J. Cancer* **90**(11), 2118–2122 (2004).
4. V. Ntziachristos and B. Chance, "Probing physiology and molecular function using optical imaging: applications to breast cancer," *Breast Cancer Res. Treat.* **3**(1), 41–46 (2001).
5. D. Grosenick, K. T. Moesta, M. Moller, J. Mucke, H. Wabnitz, B. Gebauer, C. Stroszczynski, B. Wassermann, P. M. Schlag, and H. Rinneberg, "Time-domain scanning optical mammography. I. Recording and assessment of mammograms of 154 patients," *Phys. Med. Biol.* **50**(11), 2429–2449 (2005).
6. P. Taroni, A. Torricelli, L. Spinelli, A. Pifferi, F. Arpaia, G. Danesini, and R. Cubeddu, "Time-resolved optical mammography between 637 and 985 nm: clinical study on the detection and identification of breast lesions," *Phys. Med. Biol.* **50**(11), 2469–2488 (2005).
7. S. G. Orel and M. D. Schnall, "MR imaging of the breast for the detection, diagnosis, and staging of breast cancer," *Radiology* **220**(1), 13–30 (2001).
8. M. V. Knopp, H. von Tengg-Kobligk, and P. L. Choyke, "Functional magnetic resonance imaging in oncology for diagnosis and therapy monitoring," *Mol. Cancer Ther.* **2**(4), 419–426 (2003).
9. A. A. Oraevsky, R. O. Esenaliev, S. L. Jacques, F. K. Tittel, and D. Medina, "Breast cancer diagnostics by laser optoacoustic tomography," in *Trends in Optics and Photonics*, R. R. Alfano and J. G. Fujimoto, Eds., pp. 316–321, OSA Publishing House, Washington, DC (1996).
10. A. A. Oraevsky, A. A. Karabutov, S. V. Solomatin, E. A. Savateeva, V. G. Andreev, Z. Gatalica, H. Singh, and D. R. Fleming, "Laser optoacoustic imaging of breast cancer *in vivo*," *Proc. SPIE* **4256**, 6–15 (2001).
11. V. G. Andreev, A. A. Karabutov, S. V. Solomatin, E. V. Savateeva, V. Aleynikov, Y. V. Zhulina, R. D. Fleming, and A. A. Oraevsky, "Optoacoustic tomography of breast cancer with arc-array transducer," *Proc. SPIE* **3916**, 36–47 (2000).
12. A. A. Oraevsky, V. G. Andreev, A. A. Karabutov, and R. O. Esenaliev, "Two-dimensional opto-acoustic tomography: transducer array and image reconstruction algorithm," *Proc. SPIE* **3601**, 256–267 (1999).
13. R. A. Kruger, D. R. Reinecke, and G. A. Kruger, "Thermoacoustic computed tomography-technical considerations," *Med. Phys.* **26**(9), 1832–1837 (1999).
14. R. O. Esenaliev, A. A. Karabutov, and A. A. Oraevsky, "Sensitivity of laser opto-acoustic imaging in detection of small deeply embedded tumors," *IEEE J. Sel. Top. Quantum Electron.* **5**(4), 981–988 (1999).
15. S. Manohar, S. E. Vaartjes, J. C. G. van Hespen, J. M. Klaase, F. M. van den Engh, W. Steenbergen, and T. G. van Leeuwen, "Initial results of *in vivo* noninvasive cancer imaging in the human breast using near-infrared photoacoustics," *Opt. Express* **15**(19), 12277–12285 (2007).
16. G. Ku, B. D. Fornage, X. Jin, M. Xu, K. K. Hunt, and L. V. Wang, "Thermoacoustic and photoacoustic tomography of thick biological tissues toward breast imaging," *Technol. Cancer Res. Treat.* **4**(5), 559–566 (2005).
17. D. Grosenick, H. Wabnitz, K. T. Moesta, J. Mucke, P. M. Schlag, and H. Rinneberg, "Time-domain scanning optical mammography. II. Optical properties and tissue parameters of 87 carcinomas," *Phys. Med. Biol.* **50**(11), 2451–2468 (2005).
18. A. Cerussi, N. Shah, D. Hsiang, A. Durkin, J. Butler, and B. J. Tromberg, "*In vivo* absorption, scattering, and physiologic properties of 58 malignant breast tumors determined by broadband diffuse optical spectroscopy," *J. Biomed. Opt.* **11**(4), 044005 (2006).
19. W.-F. Cheong, S. A. Prahl, and A. J. Welch, "A review of the optical properties of biological tissues," *IEEE J. Quantum Electron.* **26**(12), 2166–2185 (1990).
20. A. A. Oraevsky, S. L. Jacques, and F. K. Tittel, "Measurement of tissue optical properties by time-resolved detection of laser-induced transient stress," *Appl. Opt.* **36**(1), 402–415 (1997).
21. G. J. Diebold, M. I. Khan, and S. M. Park, "Photoacoustic "signatures" of particulate matter: optical production of acoustic monopole radiation," *Science* **250**(4977), 101–104 (1990).
22. G. J. Diebold, T. Sun, and M. I. Khan, "Photoacoustic monopole radiation in one, two, and three dimensions," *Phys. Rev. Lett.* **67**(24), 3384–3387 (1991).
23. S. A. Ermilov, A. Conjusteau, K. Mehta, R. Lacewell, P. M. Henrichs, and A. A. Oraevsky, "128-channel laser optoacoustic imaging system (LOIS-128) for breast cancer diagnostics," *Proc. SPIE* **6086**, 68–80 (2006).
24. R. A. Kruger, P. Liu, Y. R. Fang, and C. R. Appledorn, "Photoacoustic ultrasound (PAUS)—reconstruction tomography," *Med. Phys.* **22**(10), 1605–1609 (1995).
25. K. P. Kostli, M. Frenz, H. Bebie, and H. P. Weber, "Temporal backward projection of optoacoustic pressure transients using Fourier transform methods," *Phys. Med. Biol.* **46**(7), 1863–1872 (2001).
26. M. Xu and L. V. Wang, "Time-domain reconstruction for thermoacoustic tomography in a spherical geometry," *IEEE Trans. Med. Imaging* **21**(7), 814–822 (2002).
27. V. G. Andreev, A. A. Karabutov, and A. A. Oraevsky, "Detection of ultrawide-band ultrasound pulses in optoacoustic tomography," *IEEE Trans. Ultrason. Ferroelectr. Freq. Control* **50**(10), 1383–1390 (2003).
28. *American National Standard for Safe Use of Lasers*, ANSI, Washington, DC (2000).
29. G. S. Kino, *Acoustic Waves: Devices, Imaging, and Analog Signal Processing*, Prentice-Hall, Englewood Cliffs, NJ (1987).
30. A. A. Oraevsky and A. A. Karabutov, "Optoacoustic tomography," in *Biomedical Photonics Handbook*, T. Vo-Dinh, Ed., pp. 34/31–34/34, CRC Press, Boca Raton, FL (2003).
31. J. Mobley and T. Vo-Dinh, "Optical properties of tissue," in *Biomedical Photonics Handbook*, T. Vo-Dinh, Ed., pp. 2/1–2/75, CRC Press, Boca Raton, FL (2003).
32. F. A. Duck, *Physical Properties of Tissue: A Comprehensive Reference Book*, Academic Press, London (1990).
33. T. D. Khokhlova, I. M. Pelivanov, V. V. Kozhushko, A. N. Zharinov, V. S. Solomatin, and A. A. Karabutov, "Optoacoustic imaging of absorbing objects in a turbid medium: ultimate sensitivity and appli-

cation to breast cancer diagnostics," *Appl. Opt.* **46**(2), 262–272 (2007).
34. I. Patrikeev and A. A. Oraevsky, "Multiresolution reconstruction method to optoacoustic imaging," *Proc. SPIE* **4960**, 99–105 (2003).
35. G. Strang and T. Nguyen, *Wavelets and Filter Banks*, Wellesley-Cambridge Press, Wellesley, MA (1996).
36. S. A. Ermilov, R. R. Gharieb, A. Conjusteau, T. Miller, K. Mehta, and A. A. Oraevsky, "Data processing and quasi-3D optoacoustic imaging of tumors in the breast using a linear arc-shaped array of ultrasonic transducers," *Proc. SPIE* **6856**, 685603 (2008).
37. L. Wang, S. L. Jacques, and L. Zheng, "MCML—Monte Carlo modeling of light transport in multi-layered tissues," *Comput. Methods Programs Biomed.* **47**(2), 131–146 (1995).
38. T. Khamapirad, P. M. Henrichs, K. Mehta, T. Miller, A. Yee, and A. a. Oraevsky, "Diagnostic imaging of breast cancer with LOIS: clinical feasibility," *Proc. SPIE* **5697**, 35–44 (2005).
39. M. Xu and L. V. Wang, "Universal back-projection algorithm for photoacoustic computed tomography," *Phys. Rev. E* **71**(1, Pt 2), 016706 (2005).
40. L. Spinelli, A. Torricelli, A. Pifferi, P. Taroni, G. Danesini, and R. Cubeddu, "Characterization of female breast lesions from multi-wavelength time-resolved optical mammography," *Phys. Med. Biol.* **50**(11), 2489–2502 (2005).
41. A. Rice and C. M. Quinn, "Angiogenesis, thrombospondin, and ductal carcinoma *in situ* of the breast," *J. Clin. Pathol.* **55**(8), 569–574 (2002).
42. G. N. Naumov, L. A. Akslen, and J. Folkman, "Role of angiogenesis in human tumor dormancy: animal models of the angiogenic switch," *Prog. Cell Cycle Res.* **5**(16), 1779–1787 (2006).
43. L. R. Hirsch, A. M. Gobin, A. R. Lowery, F. Tam, R. A. Drezek, N. J. Halas, and J. L. West, "Metal nanoshells," *Ann. Biomed. Eng.* **34**(1), 15–22 (2006).
44. G. Ku and L. V. Wang, "Deeply penetrating photoacoustic tomography in biological tissues enhanced with an optical contrast agent," *Opt. Lett.* **30**(5), 507–509 (2005).
45. X. Huang, I. H. El-Sayed, W. Qian, and M. A. El-Sayed, "Cancer cell imaging and photothermal therapy in the near-infrared region by using gold nanorods," *J. Am. Chem. Soc.* **128**(6), 2115–2120 (2006).
46. Y. H. Berthelot and I. J. Busch-Vishniac, "Laser-induced thermoacoustic radiation," *J. Acoust. Soc. Am.* **78**(6), 2074–2082 (1985).
47. R. Simmons, "Ultrasound in the changing approaches to breast cancer diagnosis and treatment," *Breast J.* **10**(Suppl 1), S13–14 (2004).
48. G. J. Diebold and T. Sun, "Properties of photoacoustic waves in one, two, and three dimensions," *Acustica* **80**, 339–351 (1994).